Relative performance of metal and polymeric foam sandwich plates under low velocity impact

A Rajaneesh, I Sridhar* and S Rajendran

School of Mechanical and Aerospace Engineering, 50 Nanyang Avenue,
Nanyang Technological University, Singapore 639798, Singapore.

*corresponding author Email: msridhar@ntu.edu.sg

ABSTRACT

Relative performance of metal and polymeric foam cored sandwich plates is studied under low velocity impact loading. The metal foam sandwich plate is constructed using aluminum alloy foam (Alporas) core of 40 mm thickness (with two layers of 20 mm each) and aluminum faceplates. The polymeric foam sandwich plate is constructed using polyvinyl chloride (Divinycell H80 and H250) foam core of same thickness and same aluminum faceplates. Impact experiments are conducted with a hemispherical punch of mass 8.7 kg at a nominal velocity of 5.8 m/s. The effect of stepwise core grading on the maximum dynamic penetration force as well as energy absorption is studied. To maximize the energy absorption or to minimize the mass of the sandwich plate for a given penetration force, alternatives to Alporas foam are chosen based on either equivalent density (H250) or through-thickness compressive yield strength (H80). The increase in penetration force and energy absorption resulting from the choice of H250 in place of Alporas for the same density of the foam as well as the effect of decrease in mass of the sandwich panel by choosing H80 foam in place of Alporas for the same yield strength of the foam is discussed. Numerical models were developed in LS-Dyna to predict the impact response (force-displacement history) and failure modes. Upperbound analytical equations are used to estimate the maximum penetration force. Close agreement is observed between analytical estimates, experimental measurements and numerical predictions.

Keywords: Al alloy and PVC foams, graded core, FE modeling, low velocity impact, energy absorption.

1 Introduction

Naturally available cellular structures such as balsa wood, bone have high specific strength and stiffness. Recently both engineering alloys and polymers have been foamed to a range of relative densities by a variety of manufacturing processes [1, 2]. These foams are utilized as cores in sandwich construction with strong and stiff faceplates designed against static indentation (loading rates of $<$1 /s), low (5-10 /s) or high (10^2-10^5 /s) velocity impact and blast loading conditions [3–6].

Mines et al. [7] conducted a series of impact tests on two types of sandwich plates (woven glass vinyl ester skin/Coremat core and woven glass epoxy skin/honeycomb core) and concluded that perforation energy can be increased by using ductile skins and use of multiple layers of the core. Zhao et al. [8] have modified the split-Hopkinson pressure bar to measure the impact response of aluminum alloy foam (CYMAT) sandwich plates up to a velocity of 50 m/s. Akil Hazizan and Cantwell [9] conducted impact tests on sandwich plates with woven glass phenolic resin faceplate and three types of polymeric foams as cores (linear PVC, polyetherimide or PVC/PUR foam). They observed shear cracking of core, fiber buckling close to impact and delamination in the top faceplate as dominant failure patterns. More recently, Zhou et al. [10] conducted normal and oblique impact tests on a range of densities of bare foams and sandwich plates (with linear PVC, cross-linked PVC or PET foams from Airex AG). They found that the cross-linked PVC foams offered a higher perforation resistance than linear PVC foams at low densities, whereas the converse is true for higher density foams. Experimental observations on bare foams revealed a combination of pure core shear and conoid failure modes.

Expensive experimental methodologies can be replaced by approximate analytical models for design purposes. Hoo-Fatt and Park [11] provided an upper bound estimates for the peak load of sandwich plates subjected to low velocity impact. The authors considered face failure by shear (under flat punch) or tensile failure of face (under hemispherical punch), core shear and bottom faceplate failure as dominant failure modes. Olsson [12] proposed a method for predicting the small/large mass impact response and damage of composite sandwich plates accounting for local core crushing, delamination and large face sheet deflections without any empirical constants in the contact law. Semi-analytical methods are used to predict the force-displacement history under large mass impact, in which contact between plate and impactor is modelled by a linear or nonlinear spring [13, 14].

Experimental evaluation of impact response on a variety of sandwich plates is costly and time consuming, and approximations in analytical models can be avoided by using detailed numerical models. Appropriate numerical models can accurately predict the impact force-displacement histories and failure modes. A detailed description of the numerical modeling strategies available in literature is provided in [15].

It is important to investigate the relative performance of the foams so as to minimize the weight of the sandwich panel for a given energy absorption capacity or to maximize the energy absorption for a given mass under prescribed loading conditions. Relative performance of sandwich plates with Alporas® and Divinycell® PVC foams is studied by Compston et al. [16]. Faceplates for Alporas and PVC foam sandwich plates are constructed using lamina of 754 gsm (plain weave glass fiber/polypropylene prepreg) and 450 gsm (plain weave glass fiber/vinylester resin matrix using wet lay-up), respectively. However, the overall fiber content in each sandwich structure is maintained approximately the same and the authors concluded that PVC foam sandwich plates have smaller overall deflection against Alporas sandwich plates. Relative performance of motorcycle helmet with aluminum alloy foam (Alulight) shell against ABS polymeric shell is studied by Pinnoji et al. [17] and concluded that the resultant force on the head is small in case of low density metal foam helmet. Crupi et al. [18] investigated the relative performance of the GFRP/PVC foam (75 kg/m^3) sandwich plate against two types of aluminum alloy sandwich plates (from Schunk GmbH and Alulight GmbH) and concluded that PVC foam sandwich plates require high energy compared to aluminum alloy sandwich panels. However, in the attempts reported in literature for relative performance evaluation, the sandwich panels do not consists of same type of faceplate materials.

In contrast to the conventional sandwich construction with single core layer, several layers of foams are often used in recent literature to increase the energy absorption capacity. Zeng et al. [19] investigated the perforation of two core gradient varieties (viz., monotonically ascending density and monotonically descending density) in sandwich plate using four different densities of polyepoxide hollow spheres layers. Authors concluded that ascending density configuration has shown higher energy absorptions with low damage initiation force against descending density configuration. Yang and Qiao [20] have used two layers of aluminum honeycomb core sandwich structures to protect highway bridge girders under low velocity impact loading. Gardner et al. [21] used stepwise graded core with two layers, three layers, and four layers of foam core gradation to monotonically increase the acoustic wave impedance of sandwich plate in testing the blast resistance of sandwich structures using shock-tube apparatus. Experimental results showed that monotonic increase in number of graded layers increases the blast resistance of the structure. To the best of

authors knowledge, a comprehensive relative performance evaluation and failure modes comparison between PVC (Divinycell H grade) and aluminum alloy foam (Alporas) and effect of core grading have not been reported in literature. Hence, a detailed evaluation of relative performance and effect of core grading of Alporas and Divinycell PVC foams under low velocity impact is the focus of the present work using experimental and numerical studies.

In the present work, relative performance of sandwich plates consisting of Divinycell PVC and Alporas (ALP) foam core with aluminum faceplates is studied under low velocity impact. For a meaningful comparison, H80 and H250 are selected with yield strength and density equal to that of Alporas foam: H80 has same yield strength as that of Alporas foam and H250 has same mass density as that of Alporas. Effect of core grading on maximum dynamic penetration force and energy absorption capacity is also investigated by interchanging the layers of H80, H250 and Alporas foams. Using numerical models, failure modes and impact force-displacement response are predicted and compared with that of experiments. Upperbound analytical calculations were used to estimate the penetration force.

2 Methodology

2.1 Analytical modeling

In this section, analytical models for estimating the peak force (under low velocity impact) are summarized from literature.

2.1.1 Analytical modeling of bare foam impact

Flores-Johnson and Li [22, 23] investigated the indentation and low velocity impact response of polymethacrylimide (PMI) and polyetherimide (PEI) foams using different geometry of punches and proposed an analytical estimate for indentation load-displacement relation. These estimates will be used in present work.

When elastic-perfectly plastic foam experiences impact with a spherical punch, the impact force-displacement curve has a plateau region when the indentation depth is equal to the punch radius. An approximate analytical estimate for this plateau force (under spherical impactor) is expressed as [22]

$$P_{plateau} = P_{crushing} + P_{tearing} + P_{friction} \quad (1)$$

$$P_{plateau} = \pi R_i^2 \sigma_{y_c} + 2\pi R_i \gamma_c + \frac{\pi^2}{2} R_i^2 \mu \sigma_{y_c} \quad (2)$$

where, R_i is the impactor hemispherical nose radius, σ_{y_c} is the yield strength of the core, γ_c is the tear energy of the core and μ is the coefficient of friction between the foam and the indentor. More details about the impact force-displacement curve characteristics will be discussed in section 3.2.1.

2.1.2 Analytical modeling of sandwich impact

Upper bound calculations for the penetration force estimates is summarized here from the work of Hoo-Fatt and Park [11]. Top faceplate damage initiation occurs by its tensile failure involving membrane stretching. Schematic diagram of a typical shear plug failure mode is shown in Fig. 1. Penetration force (P_f) for a sandwich plate with linear elastic perfectly plastic faceplate and perfectly plastic core can be expressed as follows:

$$P_f = 2\sqrt{2}\pi R_e \frac{E_f h_f}{(1-\nu_f{}^2)} \varepsilon_f{}^{3/2} + \pi K_c R_e{}^2 \sigma_{y_c} + 2\pi R_i \gamma_c \quad (3)$$

where, h_f, E_f, ν_f and ε_f are the thickness, Young's modulus, Poisson's ratio and dynamic fracture strain of the faceplate material, respectively, R_e is the effective radius of the hemispherical impactor nose and K_c is the constraint factor for core crushing. In the work of Hoo-Fatt and Park [11], R_e is taken as 0.4 times the radius of the impactor, and K_c is chosen as 2.0 (an average value from a range between 1.7 and 2.5, based on the compression and indentation tests of Wen et al. [24]).

2.2 Experimental investigation

This section discusses the details about materials and their characterization, specimen geometries and loading conditions used in the impact experiments.

2.2.1 Materials characterization

Alporas foams and H80 and H250 foams were used in present study. Alporas is a closed cell aluminum alloy foam manufactured by Shinko Wire Co., Japan. The relative density of Alporas used in present study has 8.5% with an average cell size of 4.7 mm. PVC foams of grades H80 and

H250 are closed cell foams manufactured by Diab Inc. The numeric part in the nomenclature of the foams represents the nominal density (i.e. H80 and H250 have densities of 80 kg/m^3 and 250 kg/m^3, respectively). However, the measured average densities of H80 and H250 foams were 68 kg/m^3 and 230 kg/m^3 with an average cell size of 0.4 mm and 0.15 mm, respectively. Half-hard cold worked aluminum sheets of thicknesses 0.5 mm and 1.0 mm were used as faceplate materials for sandwich plate construction.

Tensile tests were performed on dog-bone specimens of aluminum sheets and PVC foams prepared according to ASTM E8-04 and ISO 527, respectively. Alproas foam was also cut according to ASTM E8-04 with a minimum of seven cells in the gauge length to avoid cell size effects. The dogbone samples were gripped using wedge grips for Al faceplates, and mechanical side grips for PVC and Alporas foams. Clip-on extensometer (Instron 2630-100 series with 50 mm gauge length) was used to measure the strain during tensile testing. Uniaxial tension tests were performed using Instron 5500R universal testing machine with a displacement loading at 1 mm/min. Uniaxial tensile stress-strain response of aluminum sheets and foams is shown in Figs. 2a and 2b, respectively. From the tensile tests of aluminum sheet material (in length, width and 45° directions), it was confirmed to be nearly isotropic with elastic-perfectly plastic behavior. The effect of aluminum sheet thickness on Young's modulus value is found to be negligible. However, the yield strength increased up to 12 % with an increase in aluminum sheet thickness from 0.5 mm to 1.0 mm. The tensile modulus of Alporas foam is higher than that of PVC foams; however the failure stress and strain are lesser than that of PVC foams as shown in Fig. 2b.

Compression tests on PVC foams were performed using 30 mm thick specimens with in-plane dimensions 50 mm x 50 mm, where as for Alporas foam a cuboid of 50 mm side length was used to avoid the size effects (minimum dimension of the specimen should be at least seven times the cell size) of the Alporas foam. Compression strain was calculated from the cross head displacement. Loading and unloading cycles were used in compression test to measure the corresponding loading and unloading modulus of the foams. Daniel and Cho [25] have shown that the through-thickness and in-plane compression properties differ and hence orthotropy needs to be considered for PVC foams. To account for orthotopy, compression tests were performed in through-thickness and in-plane (length and width) directions. The uniaxial compression test response of different foams tested is shown in Fig. 3. Compression response of H250 and H80 shows that, the through-thickness strength is higher than in-plane strength (by a factor of 1.6 for H80 and 1.3 for H250). It was observed that the in-plane compressive strengths of H80 and H250 foams in length and width directions are close enough. However, the compression modulus of H250 foam in length direction is smaller in comparison to that in width direction, whereas H80 foam shows in-plane isotropy. The

yield strengths of H80 and Alporas foams are almost the same (1.5 MPa for Alporas and 1.2 MPa for H80), however the rate of densification (change in stress with respect to change in strain) of Alporas foam is quite fast compared to that of H80 foam. Though the cell size of Alporas foam is larger than H80 foam, the fast rate of densification observed is due to cell wall material constitutive property.

2.2.2 Impact testing

Sandwich plates with in-plane dimensions 100 mm x 100 mm were fabricated by bonding aluminum faceplates to 40 mm thick foam layers. The faceplates on both sides of the core were either of thickness 0.5 mm or 1.0 mm. Two foam layers (viz., Alporas, H80 or H250) each of thickness 20 mm were bonded to give 40 mm thick core. PVC foam samples with in-plane dimensions 100 mm x 100 mm were cut from a foam block using circular saw and Alporas foam specimens were cut using electrical discharge machining (EDM) to minimize the damage to the cell walls.

Bonding between various interfaces was achieved using two-part methacrylate structural adhesive, MA310 (from ITW Plexus). Typical cured MA310 adhesive has an Young's modulus of 1.1 GPa, failure stress of 20 MPa, and failure strain of 10 % [26]. These properties ensure no premature failure of adhesive interface under low speed impact loading conditions. To maintain constant bondline thickness, a fiber glass mesh of 0.2 mm thickness was used at all the bonding interfaces.

To understand the contributions of each constituents of the sandwich plate, impact tests were carried out on the aluminum sheets and foams of thickness 20 mm and 30 mm, and bare graded foams of thickness 40 mm in addition to the tests on sandwich plates. For effective comparison, H80 and H250 were selected against Alporas foam because H80 and Alporas foam have approximately the same yield strength whereas H250 and Alporas foam have approximately the same density. As an additional objective, the effect of core grading on impact response (peak force and energy absorption) is investigated.

All the impact tests were performed using Instron Dynatup 9250 apparatus with an impactor of 8.7 kg mass at 5.8 m/s velocity. Details of the experimental setup are discussed in the work of Mohan et al. [27]. Sandwich plate is clamped using two pneumatic plates (of size 100 mm x 100 mm with central circular hole of diameter 76 mm) on the top and bottom. Response from the impactor (tup) is recorded using the data acquisition system. Three set of experiments were conducted on each type bare foam specimens (20 mm and 30 mm) to ensure repeatability. The experimental scatter was found to be negligibly small. However owing to material availability constraint, only one set of experiments were conducted on 40 mm bare foams and sandwich plates. Possibility of experimental scatter and stochastic variations in the material types, adhesive amount

and any experimental scatter are thus constrained by the sample size. In this experimental study, the impact response of nine 40 mm thick foams and eighteen sandwich plate designs were investigated.

2.3 Numerical modeling

Finite element (FE) models were developed in LS-Dyna to predict the impact behavior of the sandwich plates. Owing to the symmetry, quarter models were developed for numerical simulation and symmetric boundary conditions are applied on the planes of symmetry. A typical FE model of the sandwich plate with mesh details is shown in Fig. 4. The clamped boundary conditions in the experiment were simulated by constraining all nodes around the curvilinear boundary of the plate. The mesh was refined in the vicinity of the plate center so as to keep an element aspect ratio of 1-2 (with element dimensions of 0.5 mm) while coarse mesh was used in the regions away from the impact region.

All the parts were meshed with constant stress solid element. Hourglass control was used to avoid spurious modes and care was taken to keep hourglass energy within 10% of peak internal energy value. Contact between plate and rigid punch was achieved using node to surface erosion contact option. Tie constraints were applied to simulate bonding between various interfaces. The selected adhesive ensures no interfaces de-bonding, hence tie constraint failure is not considered in the present FE model. Effect of friction between the impactor and the sandwich plate was neglected as the contact duration is very short. Excessive element distortions and smaller time steps (caused by thinning of element) were avoided by eroding elements if the time step decreases to 60% of its initial time step value.

Hemispherical impactor was modeled as a rigid body (using steel properties: Youngs modulus of 200 GPa, density of 7860 kg/m^3 and Poissons ratio of 0.3) with lumped mass of 8.7 kg and an impact velocity of 5.8 m/s using PART_INERTIA card. Aluminum faceplates were modeled using piece-wise linear plasticity material with J_2-flow theory and isotropic hardening (MAT_PIECEWISE_LINEAR_PLASTICITY, MAT_24). Input material properties of aluminum faceplate are listed in Table 1. Core materials (Alporas, H80 and H250) were modeled using homogenized honeycomb model (MAT_HONEYCOMB, MAT_26). In this constitutive model, orthotropic foams can be modeled by defining different compression stress-strain curve in different directions. However, in homogenized honeycomb model coupling between the stress components is not considered. The material property values used for simulating Alporas, H80 and H250 foams are listed in Tables 2, 3 and 4, respectively. The loading modulus value measured from the present experiments is 300 MPa (from 50 mm thick specimens). However, Ramamurty and Paul [28] observed certain variability in the loading modulus of foams with respect to thickness of foams. Mean

loading modulus values for 25 mm, 50 mm and 115 mm thick foams was reported as 180 MPa, 290 MPa and 460 MPa, respectively. In present work Alporas foams under investigation are of thickness 20 mm, hence Alporas foam was modeled with a Young's modulus of 180 MPa.

For Alporas foam, always maximum strain failure criterion was used irrespective of its location in graded construction. However, for PVC foams H80 and H250, maximum strain failure criterion was used as long as there exists any backing layer. Otherwise, tensile volumetric strain ($\varepsilon_{11} + \varepsilon_{22} + \varepsilon_{33}$) criterion [29] was used with MAT_ADD_EROSION option. Similar failure mode was simulated by Zhou et al. [10] using hydrostatic stress criterion. For example, in H80/H80 bare foam impact simulation, maximum strain criteria for the top layer of H80 and volumetric strain criterion for the bottom layer of H80 were used. These failure criterion were selected to simulate the observed failure modes. The damage parameters in the constitutive model are calibrated against experimental test data for the considered mesh size.

All computations were carried out on high performance computing cluster facility using 4 nodes, each node consists of 8 CPUs (total of 32 CPUs) using MPP capabilities of LS-DYNA (version R5.1.1). Each node has 32 GB of shared memory.

3 Results and discussion

In this section, comparison between predicted as well as observed failure modes and impact force-displacement responses are discussed followed by a comparison of different graded bare foams and sandwich designs using bar charts.

3.1 Failure modes

3.1.1 Bare foams - one layer

Impact on bare Alporas foam blank leaves a straight hole through the thickness of the foam block. However, in PVC foams, the perforation path is straight till 1/2 to 3/4th of foam blank thickness followed by conoid formation. Typical failure modes observed in experiments and that predicted using FE models, are shown in Fig. 5. Brittle materials such as glass under localized indentation loads fail by pure conical mode of cracking [30]. Under impact loading, shear plug failure mode occurs in thicker plates while tensile failure with the formation of conoid is likely to occur in thinner plates. This is because comparatively bending becomes dominant in thinner plates and the conical portion of the failure surface always occurs on the lower side of the plates where tension is developed. A combination of shear plug and conical cracking failure mode is observed in concrete

as reviewed by Li et al. [31]. The transition length from pure shear plug to cone cracking occurs when the penetration force in-front of the projectile is equal to the shear force in the remaining thickness of the concrete. Li et al. [31] also provided an empirical formula based on a large number of experiments for the shear-plug and conoid formation transition length in terms of compressive strength of the un-reinforced concrete and the ratio of target thickness (H) to projectile radius (R_i). Concrete is brittle in both tensile and compressive loading conditions, whereas cellularic PVC foams depict brittle behavior only under tensile loading due to the breaking of the cell-walls. Hence, the transition length in bear foams depends possibly on the tensile strength and H/R_i. Due to constraints on the different thicknesses of PVC foam samples and tearing energy data as a function of foam relative density, obtaining an empirical equation for the transition length for shear plug to conical mode of failure in these polymeric foams is beyond the scope of this paper. The base of the conoid (cone-shaped shear plug) observed in the experiments was neither circular nor elliptic but arbitrary in shape owing to orthotropy and inhomogeneity of the foams. Formation of the conoid is also observed in the works of Flores-Johnson and Li [22] during their indentation tests on the PEI closed-cell rigid foams (Airex R82.80) with hemispherical punch.

Length of the conoid, L_c (as shown in Fig. 5) of H80 and H250 foams was found to be 6 mm and 10 mm, respectively. Impact tests on 20 mm and 30 mm thickness samples (viz., H80 and H250) revealed that L_c does not depend on the thickness of the foam but depend on the foam density under impact. Diameter of the conoid, D_c (chord length of an arbitrary conoid) of H80 was found to vary from 20 mm to 25 mm and that of H250 was found to vary from 25 mm to 40 mm due to in-plane orthotropy of the PVC foams. Accurate prediction of arbitrary conoid shapes is not possible owing to the fact that unavailability of constitutive model for orthotropic foams accounting for the interaction between stress components. Estimated angle of the conoid of H80 was found to vary from 30° to 54° and that of H250 was found to vary from 30° to 53°.

Numerically simulated failure zone diameter for Alporas foam is in fairly good agreement with that of the experimental measurements. The diameter of the conoid, D_c of H80 foam in experiments was measured to be varying from 20 mm to 24 mm (from three repeated experiments) against 22 mm and 26 mm (in two orthotropic directions x and y) predicted by the FE model. The D_c for H250 foam was measured to be varying from 35 mm to 40 mm (from three repeated experiments) against the FE prediction of 29 mm and 33 mm (in two orthotropic directions x and y). Experimentally observed length of the shear-plug of Alporas foam is very small because of the collapse or densification due to large cell size. In PVC foams, length of the conoid is of the order of foam blank thickness due to lower densification of the foam resulting from smaller cell size as shown in Fig. 5. Numerically predicted length of the shear plugs, L_c were not in agreement with that of the

experiments because in numerical simulation elements get compressed and eroded based on stable time increment (to avoid very small time step).

3.1.2 Bare graded foams - two layers

The cut section views of bare graded foams in Fig. 6 shows the failure modes observed in test specimens. Alporas foam always fails by shear plug formation irrespective of its location in the graded construction. Failure mode of PVC foam layer depends on its location in graded construction. If a PVC foam layer is followed by stronger backing layer, then the front PVC foam layer fails by pure shear plug failure mode and the conoidal fracture is either completely absent or small. In H80/H80, H250/H250, H80/ALP and H80/H250 specimens, top layers fail by pure shear plug formation because of the presence of a backing layer of equal or higher strength. In H250/ALP specimen, the rear layer (Alporas) is low in strength, so the conoidal fracture is present in front layer (H250) while the failure in Alporas is pure shear plug with diameter equal to the conoid diameter in H250 core (see Fig. 6e). Typical shear plugs and conoid fragments are shown in Fig. 7.

3.1.3 Sandwich plates

All sandwich plates tested failed by through-hole shearing except those with 0.5 mm faceplate and H250 foam as a second layer (viz., H250/H250, H80/H250 and ALP/H250). Since aluminum faceplates with 0.5 mm thickness is not sufficient enough to act as a stiff backing for H250 foam, conoid formation has occurred. Experimental failure modes for H250/H250 sandwich plate with 1.0 mm and 0.5 mm faceplates are shown in Fig. 8. In numerical simulations, a layer of elements between bottom faceplate and core failed without any visible failure in the bottom faceplate. Sizes of the conoid in 0.5 mm and 1.0 mm sandwich plates were not accurately predicted by the present numerical models. Prediction of accurate conoid size is possible by careful calibration of erosion parameters, which in turn depend on the mesh size. A small conoid formation is observed in 1.0 mm faceplates experiments (as shown in Fig.8b) is possibly due to foam orthotropy.

3.2 Impact response: Force versus displacement

3.2.1 Bare foams of 20 mm thickness

Comparison between numerically predicted and experimentally measured impact force-displacement curves are shown in Fig. 9 along with summary of mass of the foam blanks, dynamic penetration force and energy absorption values. It can be seen that, impact event (force-displacement) consists of three stages; (a) linear region: gradual increase in force as the penetration depth increases from

zero value (b) plateau region: impact force reaches a plateau value as penetration depth is equal to punch radius and force remains constant (c) failure: formation of shear plug (in Alporas) or sudden conoid formation (in H80 or H250) occurs.

When a cellular structure experiences contact with a impactor, the cell walls ahead of the impactor buckles followed by a layer-wise collapse of thin section and their propagation leading to its densification. As impact progresses, contributions of tearing of the cell walls around the loading impactor and densification effect of foam decides either increase or constant plateau force or stress.

Analytical estimation of plateau force according to Eq. (2) need tear energy of the core, γ_c. According to Olurin et al. [32], tear energy of Alporas foam is 6.7 kJ/m^2. Using material properties of Alporas from Table 2, the plateau force for Alporas foam can be calculated as 569 N (which is in close agreement with experimental measurement). Analytical plateau forces of H80 and H250 were not verified due to lack of tear energy data. From Eq. (2) it is evident that, plateau force is independent of the thickness of the foam. The same observation can be seen from the experimental data in Fig. 9, as the thickness of the H80 foams increases from 20 mm to 30 mm, there is no change in plateau force. Similar observations were noted for Alporas foams [15]. This behavior in softer foams is due to localized damage at the core surface (localization effects) dominates the thickness effects (increase in force with respect to increase in thickness of the foam) of the core. However, thickness effect is clearly seen in H250 (strong) foam as shown in Fig. 9 against softer foams (viz., H80 and Alporas).

For a given yield strength 1.5 MPa, selecting H80 foam (of mass 13 g) in place of Alporas (of mass 45 g) leads to a decrease in maximum impact force from 0.8 kN to 0.4 kN (-50%) and a decrease in energy absorption from 9.8 J to 4.2 J (-57%). This is because the Young's modulus of the Alporas foam is higher than that of H80 foam. For a given density of 250 kg/m^3, choosing H250 in place of Alporas foam results an increase in maximum impact force from 0.8 kN to 2.6 kN (+225%) and an increase in energy absorption from 9.8 J to 26.8 J (+173%).

Correlation between the failure mode and impact force-displacement curve is evident. For Alporas foam, the failure is a through-thickness perforation, so there is no sudden drop in the force-displacement curve. Due to the formation of conoid in PVC foams, there is a sudden drop in the force-displacement curve. This sudden drop in force occurs approximately at the 1/2 to 3/4th of foam blank thickness. Although the FE models of H80 foam are able to predict the formation of conoid, the sudden drop in force-displacement curve is delayed by 4 mm as shown in Fig. 9. This delay is possibly due to the approximate nature in calibration of erosion strain value used for element deletion or due to the inability of constitutive model to account for the interaction between stress components.

3.2.2 Bare foams of thickness 40 mm

The experimentally measured impact response of bare foams of thickness 40 mm is shown in Fig. 10. Damage initiation force of 40 mm thick graded foam is governed by the top foam layer and is equal to that of front layer alone (20 mm). Effect of adhesive layer is clearly seen if both foam layers (viz., ALP/ALP, H80/H80, ALP/H80 and H80/ALP) are soft. The elastic stiffness is highest for H250/ALP panel out of all the tested panels because of the combined effect of two high Young's modulus foams (viz., Alporas and H250) considered. This ensures highest elastic energy absorption capacity and damage initiation force.

3.2.3 Sandwich plates

Sandwich plates were constructed with aluminum faceplates and Alporas foam and/or PVC foams as a core for evaluating the relative performance of Alporas foam and PVC foams. Comparison between experimental measurements and numerical predictions of force-displacement response of 0.5 mm aluminum sandwich plate is shown in Fig. 11. For a given yield strength of 1.5 MPa, replacing Alporas foam with H80 results an increase in maximum dynamic force from 1.3 kN to 1.7 kN (+30%) and correspondingly a decrease in energy absorption from 37.1 J to 32.4 J (-12.7%), a decrease in mass from 135 g to 70 g (-48%) and an increase in specific energy absorption from 0.278 kJ/kg to 0.463 kJ/kg (+66.5%). Similarly, replacing Alporas aluminum foam with H250 for a given density of 250 kg/m^3, the maximum dynamic force increases from 1.3 kN to 4.0 kN (+207%), the energy absorption increases from 37.1 J to 98.55 J(+165%) and the specific energy absorption increases from 0.278 kJ/kg to 0.725 kJ/kg (+160%). Similar trends were observed for sandwich plates with 1.0 mm faceplates with respect to maximum dynamic force and energy absorption performance values.

From the force-displacement measurements, it is obvious that the maximum dynamic force is governed by the faceplate thickness. Though the yield strength and Young's modulus of Alporas sandwich are higher than that of H80 foam, the maximum dynamic force is smaller in Alporas sandwich plate than H80 sandwich plate. This observation is consistent with sandwich plates having either 0.5 mm or 1.0 mm thick faceplates. Possible reason is due to large cell size (4.7 mm) triggering cell size effects in Alporas foam sandwich against small cell size of H80 foam (0.4 mm). However, these size effects in Alporas foam get attenuated as the faceplate thickness increases.

A comparison between numerical predictions, analytical estimates and experimental measurements is shown in Fig. 11 so as to assess the accuracy of the implemented numerical modeling methodology. For the estimation of the maximum dynamic force values using Eq. (3), material properties from Tables 1-4 were used. The failure strain of the faceplate (ε_f) used in analytical

investigation is taken from 0.5 mm thick specimen tension test data. It is evident from Fig. 7 that the shear plugs of H250 are higher (9 mm to 10 mm) in diameter compared to Alporas and H80 foams (5 mm to 6 mm). This explains that, the effective radius, R_e varies with respect to the material under impact and is higher for stronger foams. To verify this numerically, the finite element simulation output is captured (just before the maximum force) and shown in Fig. 12 for Alporas, H80 and H250 sandwich plates with 0.5 mm faceplate. It is evident that contact radius is higher for a sandwich plate with a stronger foam for a given load. Hence, for the maximum dynamic force estimation of Alporas and H80 (softer foam) sandwich plates R_e was taken as 0.4 R_i as proposed by Hoo Fatt and Park [11]. However, for H250 (strong foam based) sandwich plates R_e was estimated by geometric scaling of 0.4 R_i (based on core shear plug diameter) and a good approximate was found to be 0.75 R_i. Analytically predicted maximum penetration forces for H80 and Alporas sandwich plates are close enough as shown in Fig. 11.

3.3 Comparison charts

For effective comparison between different sandwich constituents, bare graded foams and sandwich designs, bar charts are plotted in Figs. 13 and 14 showing the maximum dynamic force, energy absorption and panel weight. Comparison chart for the sandwich constituents is shown in Fig. 13a. Thickness of the foam has no effect on the maximum dynamic force in H80 and Alporas foams because of the failure localization in the foams. However, in H250 foam, the maximum dynamic force increases with the increase in foam thickness.

Bar chart in Fig. 13b summarizes and compares the impact responses of 40 mm thick graded foams. Damage initiation force and maximum dynamic force are different in bare graded foams impact. The damage initiation force depends on type of the foam on the impact side. Soft and compliant foam on the impact side of the sandwich plate will have lower damage initiation force, with no effect on overall energy absorption (viz., H80/H250). Maximum dynamic force depends on the location of the stronger foam in the graded configuration. For a given weight; maximum dynamic force or energy absorption capacity can be improved by using H250 foam in place of Alporas foam (viz., H80/H250 instead of H80/ALP) and improved performance is obtained when the stronger foam is on the impact side (viz., H250/H80 instead of H80/H250).

Bar charts in Fig. 14 summarizes and compares the impact response of the graded sandwich plates with 0.5 mm and 1.0 mm thickness faceplates. Effect of grading sequence of softer foams is nullified in sandwich construction, i.e. ALP/H80 and H80/ALP sandwich plates have same maximum dynamic force and energy absorption capacities. Increase in faceplate thickness nullifies the effects of variation in cell size of Alporas foam and difference in moduli of softer foams (H80 and

ALP) on the maximum dynamic force and energy absorption. Using stronger foams as the front layer in graded construction increases the overall performance of the sandwich plate substantially.

4 Conclusions

The yield strength of Alporas and H80 foams does not show significant difference. However, the densification process of Alporas foam is rapid in comparison to that of H80. The in-plane strength of H80 and H250 is lower when compared to through-thickness strength. For the same weight, choosing H250 gives 300% (based on compression strength of 6.2 MPa against 1.5 MPa of Alporas) stronger structure when compared to Alporas foam structure.

Alporas foams always fail by shear plug failure mode irrespective of its location in the graded configuration. However, in PVC foams (H80 and H250), the failure mode depends on their location in the graded configuration. If a PVC foam layer is followed by an equally strong or stiff backing layer, then PVC foam fails by pure core shear plug otherwise by a combination of shear plug and conoid (conical shear plug) failure. Accurate numerical prediction of the shear plug and conoid dimensions demands a constitutive model, which considers the foam orthotropy and coupling between all the stress components.

The maximum dynamic force does not depend on the thickness of softer foams (viz., Alporas or H80) due to localized failure in softer foams. However, in dense foams (H250), the maximum dynamic force increases with the increase in thickness of the foam due to absence of localization effects. In the impact of graded bare foams, damage initiation force is governed by the top foam layer and is equal to that of front layer alone. However, the maximum dynamic force in the graded bare foam depends on the location of the stronger foam (H250) in the graded configuration.

In graded core sandwich plates, the effect of core grading can be seen only if the yield strength of the cores is different. Using cores of same yield strength in core grading has no effect on the sandwich plate performance in terms of the maximum dynamic force or energy absorption. With the use of graded core sandwich plates with thin faceplate, one can maximize the energy absorption with small maximum penetration force by using softer foam on the impact side followed by a stronger foam backing. Similarly, one can maximize the maximum dynamic force by decreasing the energy absorption value by using stronger foam on the impact side followed by softer foam. Presence of softer foams as a front layer in graded sandwich plate leads to an early triggering of indentation phenomena, so the damage initiation force is smaller in comparison to sandwich plates with stronger foams as a front layer. An increase in faceplate thickness from 0.5 mm to 1.0 mm nullifies the cell size effects of the underlying foam (viz., Alporas). Sandwich plates with H250 as

core outperform (all the other designs considered) in terms of damage initiation force and energy absorption for a given mass. The maximum penetration force predicted from numerical models and their analytical estimates are in close agreement with that of experimental measurements.

Though all the conclusions drawn on sandwich plates were based on one set of experiments, the sample size is expected to have minimal effect on repeatability, so that overall conclusions remain valid.

Acknowledgements

A Rajaneesh thanks Nanyang Technological University for the financial support in the form of Graduate Scholarship. Authors acknowledge Dr. A Ramam of IMRE, Singapore for facilitating the experiments. I Sridhar thank Temasek Laboratories @NTU for additional financial support via project No. TL9010101538-02.

References

[1] M. F. Ashby. *Metal foams : A design guide*. Butterworth-Heinemann, Boston, 2000.

[2] L. J. Gibson and M. F. Ashby. *Cellular solids : structure and properties*. Cambridge solid state science series. Cambridge University Press, Cambridge ; UK, 2nd edition, 1997.

[3] S. Abrate. Localized impact on sandwich structures with laminated facings. *Appl Mech Rev*, 50:69, 1997.

[4] J. E. Field, S. M. Walley, W. G. Proud, H. T. Goldrein, and C. R. Siviour. Review of experimental techniques for high rate deformation and shock studies. *Int J Impact Eng*, 30(7): 725–775, 2004.

[5] G. B. Chai and S. Zhu. A review of low-velocity impact on sandwich structures. *P I Mech Eng L-J Mat*, 225(4):207–230, 2011.

[6] S. Abrate, B. Castanie, and Y. D. S. Rajapakse. *Dynamic Failure of Composite and Sandwich Structures*, volume 192. Springer, 2012.

[7] R. A. W. Mines, C. M. Worrall, and A. G. Gibson. Low velocity perforation behaviour of polymer composite sandwich panels. *Int J Impact Eng*, 21(10):855–879, 1998.

[8] H. Zhao, I. Elnasri, and Y. Girard. Perforation of aluminium foam core sandwich panels under impact loadingan experimental study. *Int J Impact Eng*, 34(7):1246–1257, 2007.

[9] M. D. Akil Hazizan and W. J. Cantwell. The low velocity impact response of foam-based sandwich structures. *Compos Part B: Eng*, 33(3):193–204, 2002.

[10] J. Zhou, M. Z. Hassan, Z. Guan, and W. J. Cantwell. The low velocity impact response of foam-based sandwich panels. *Compos Sci Technol*, 2012.

[11] M. S. Hoo Fatt and K. S. Park. Dynamic models for low-velocity impact damage of composite sandwich panels - part b: Damage initiation. *Compos Struct*, 52(3-4):353–364, 2001.

[12] R. Olsson. Engineering method for prediction of impact response and damage in sandwich panels. *J Sandw Struct Mater*, 4(1):3–29, 2002.

[13] T. A. Anderson. An investigation of SDOF models for large mass impact on sandwich composites. *Compos Part B: Eng*, 36(2):135–142, 2005.

[14] I. H. Choi. Contact force history analysis of composite sandwich plates subjected to low-velocity impact. *Compos Struct*, 75(1-4):582–586, 2006.

[15] A. Rajaneesh, I. Sridhar, and S. Rajendran. Impact modeling of foam cored sandwich plates with ductile or brittle faceplates. *Compos Struct*, 94(5):1745–1754, 2012.

[16] P. Compston, M. Styles, and S. Kalyanasundaram. A comparison of low energy impact behaviour in aluminium foam and polymer foam sandwich structures. In Sandwich Structures 7: Advancing with Sandwich Structures and Materials, editor, *Thomsen, O. T. Bozhevolnaya, E. Lyckegaard, A.*, pages 643–652. Springer Netherlands.

[17] P. K. Pinnoji, P. Mahajan, N. Bourdet, C. Deck, and R. Willinger. Impact dynamics of metal foam shells for motorcycle helmets: Experiments & numerical modeling. *Int J Impact Eng*, 37(3):274–284, 2010.

[18] V. Crupi, G. Epasto, and E. Guglielmino. Low-velocity impact strength of sandwich materials. *J Sandw Struct Mater*, 13(4):409–426, 2011.

[19] H. B. Zeng, S. Pattofatto, H. Zhao, Y. Girard, and V. Fascio. Perforation of sandwich plates with graded hollow sphere cores under impact loading. *Int J Impact Eng*, 37(11):1083–1091, 2010.

[20] M. Yang and P. Qiao. Analysis of cushion systems for impact protection design of bridges against overheight vehicle collision. *Int J Impact Eng*, 37(12):1220–1228, 2010.

[21] N. Gardner, E. Wang, and A. Shukla. Performance of functionally graded sandwich composite beams under shock wave loading. *Compos Struct*, 94(5):1755–1770, 2012.

[22] E. A. Flores-Johnson and Q. M. Li. Indentation into polymeric foams. *Int J Solids Struct*, 47 (16):1987–1995, 2010.

[23] E. A. Flores-Johnson and Q. M. Li. Low velocity impact on polymeric foams. *J Cell Plast*, 47(1):45–63, 2011.

[24] H. M. Wen, T. Y. Reddy, S. R. Reid, and P. D. Soden. Indentation, penetration and perforation of composite laminate and sandwich panels under quasi-static and projectile loading. *Key Eng Mat*, 141:501–552, 1997.

[25] I. Daniel and J. M. Cho. Characterization of anisotropic polymeric foam under static and dynamic loading. *Exp Mech*, 51(8):1395–1403, 2011.

[26] ITW Plexus. Technical data sheet Plexus MA310, Rushden, UK. 2005.

[27] K. Mohan, T. H. Yip, I Sridhar, and Z. Chen. Impact response of aluminum foam core sandwich structures. *Mat Sci Eng A-Struct*, 529:94–101, 2011.

[28] U. Ramamurty and A. Paul. Variability in mechanical properties of a metal foam. *Acta Mater.*, 52(4):869–876, 2004.

[29] J. O. Hallquist. *LS-DYNA: User's manual*. Livermore software technology corporation, 1998.

[30] B. Lawn. *Fracture of Brittle Solids*. Cambridge University Press, 1993.

[31] Q. M. Li, S. R. Reid, H. M. Wen, and A. R. Telford. Local impact effects of hard missiles on concrete targets. *Int J Impact Eng*, 32(1):224–284, 2005.

[32] O. B. Olurin, N. A. Fleck, and M. F. Ashby. Indentation resistance of an aluminium foam. *Scr. Mater.*, 43:983–9, 2000.

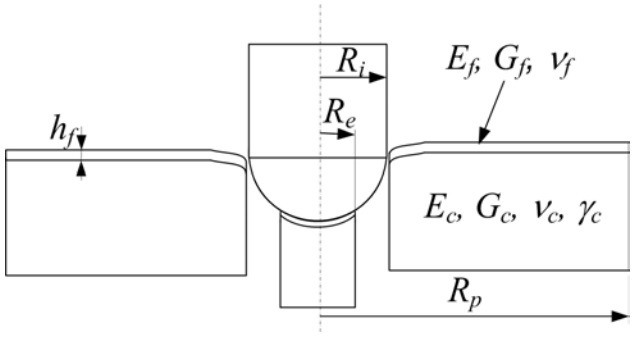

Figure 1: Failure by core shear-plug formation in ductile failure of isotropic faceplate.

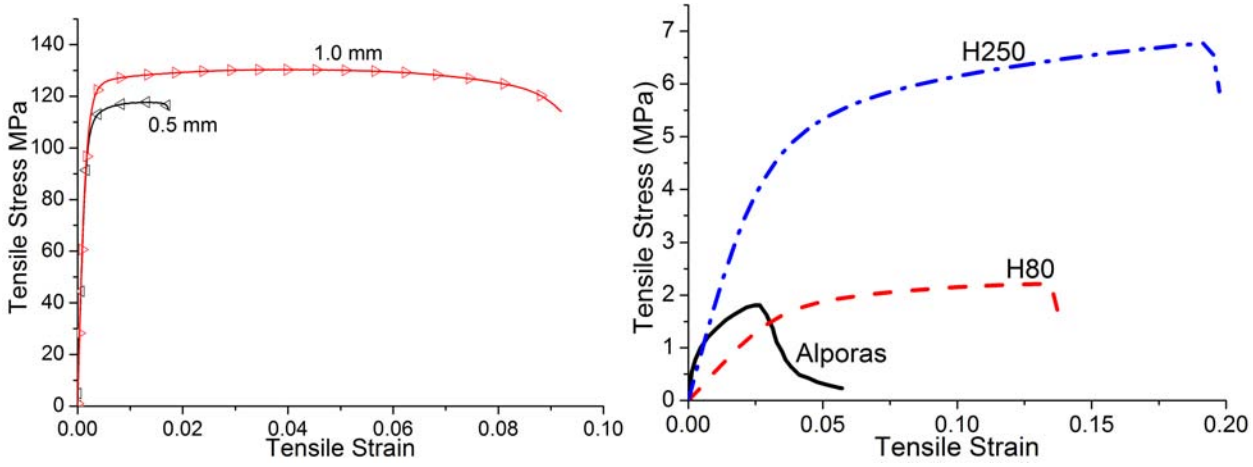

(a) (b)

Figure 2: Uniaxial tension response of (a) aluminum face sheets and (b) PVC and aluminum alloy foams.

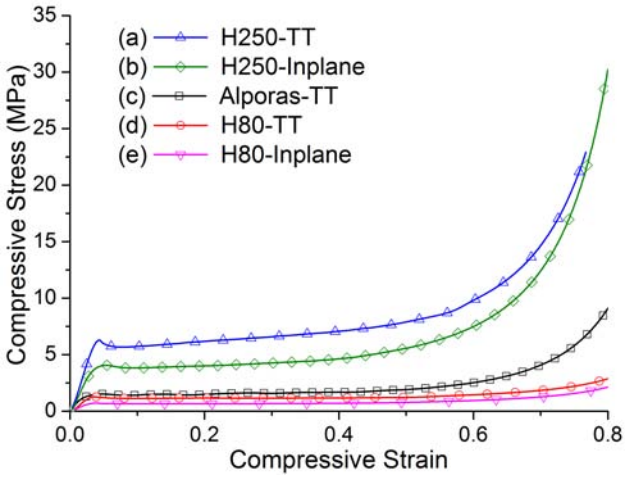

Figure 3: Uniaxial compression response of PVC and Alporas foams.

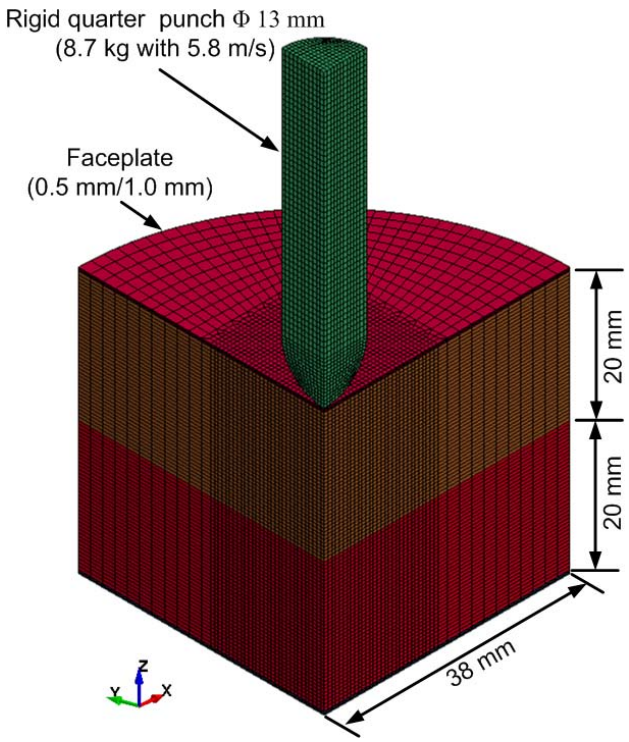

Figure 4: Quarter FE model of the graded sandwich plate. Nodes on the periphery of the sandwich plate are constrained in all directions and symmetry boundary conditions are imposed on the nodes in *xz* and *yz* plane.

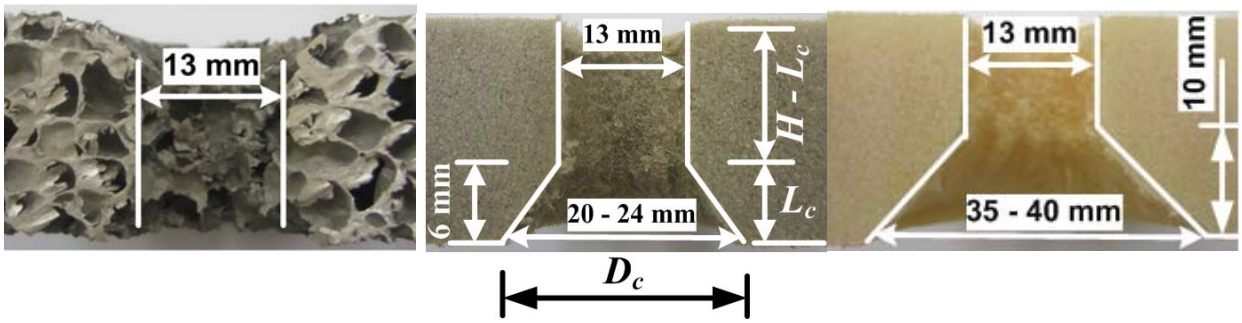

(a) Alporas experiment (b) H80 experiment (c) H250 experiment

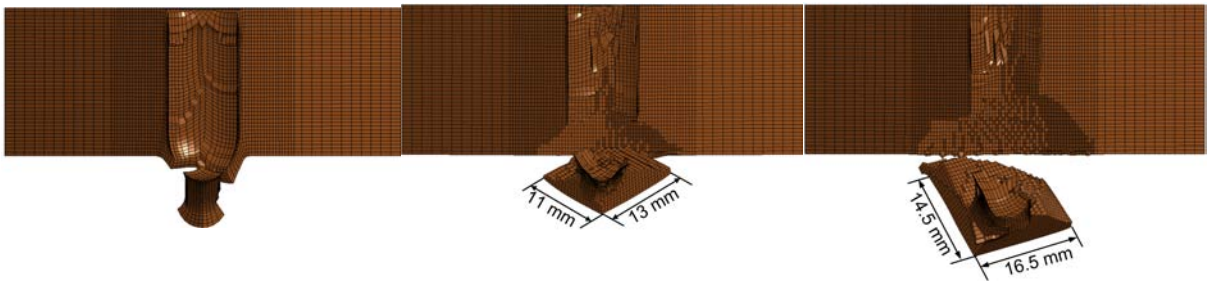

(d) Alporas FE (e) H80 FE (f) H250 FE

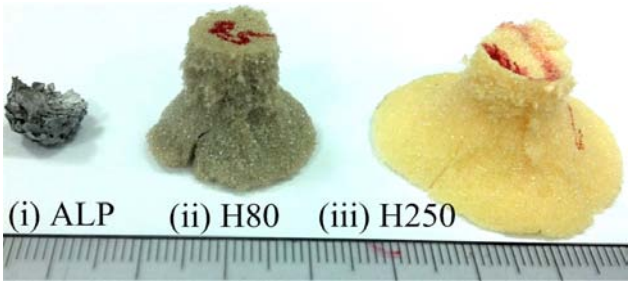

(g) Shear plugs of 20 mm foams

Figure 5: Experimental and numerical failure modes and its dimensions of 20 mm thick foams. In (b), L_c and D_c are the length and diameter of the conoid, respectively.

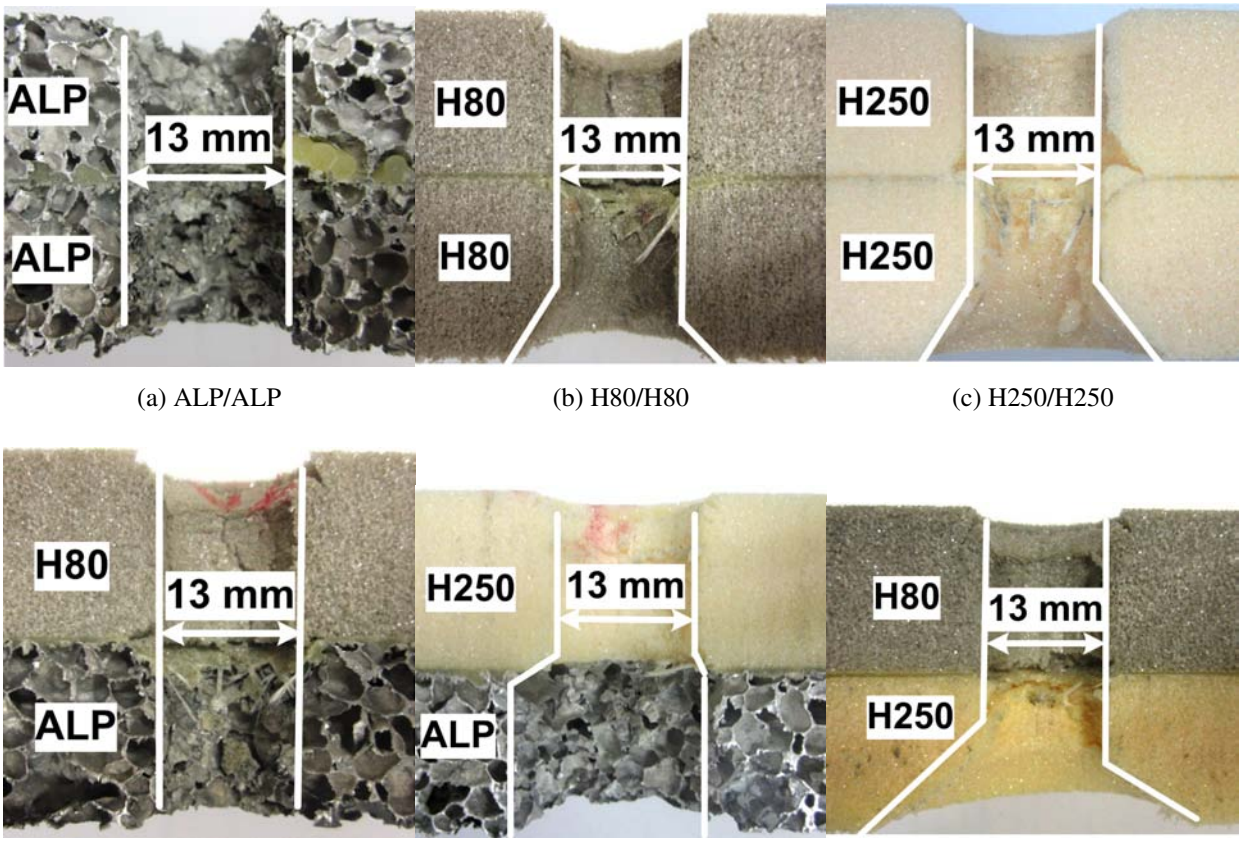

(a) ALP/ALP (b) H80/H80 (c) H250/H250

(d) H80/ALP (e) H250/ALP (f) H80/H250

Figure 6: Experimental failure modes of 40 mm thick bare foams.

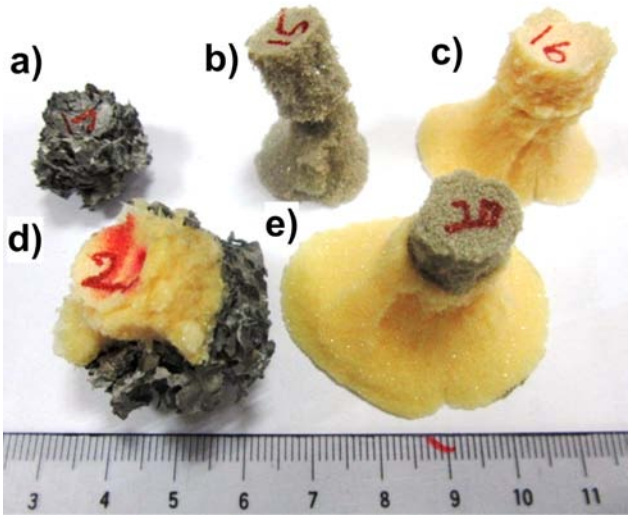

Figure 7: Typical shear plugs and conoids observed in bare graded foams. In figure (a) ALP/ALP (b) H80/H80 (c) H250/H250 (d) H250/ALP and (e) H80/H250.

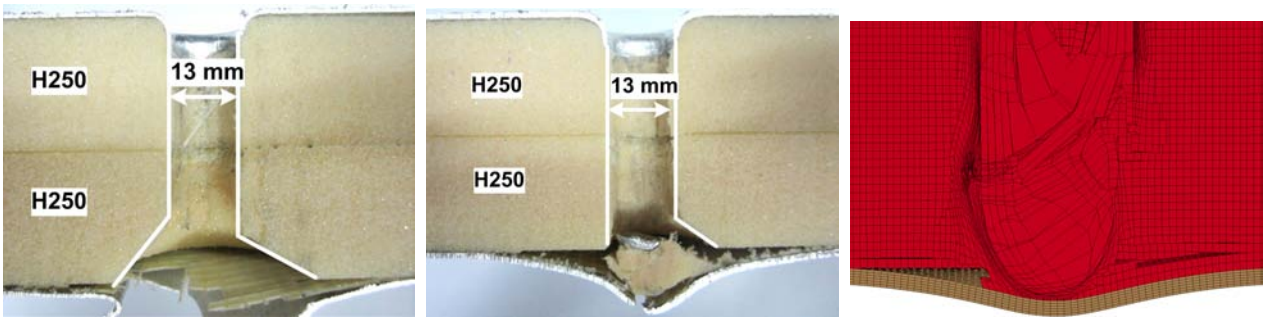

(a) Expt.: 0.5 mm (b) Expt.: 1.0 mm (c) Nume.: 1.0 mm

Figure 8: Failure modes in H250/H250 sandwich plate.

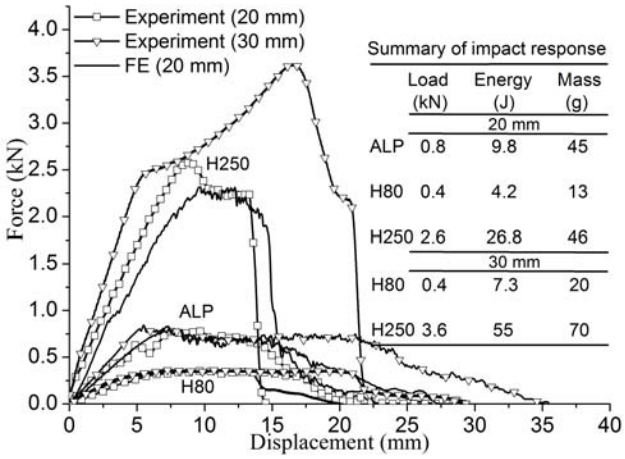

Figure 9: Force-displacement response of bare foams of thicknesses 20 mm and 30 mm.

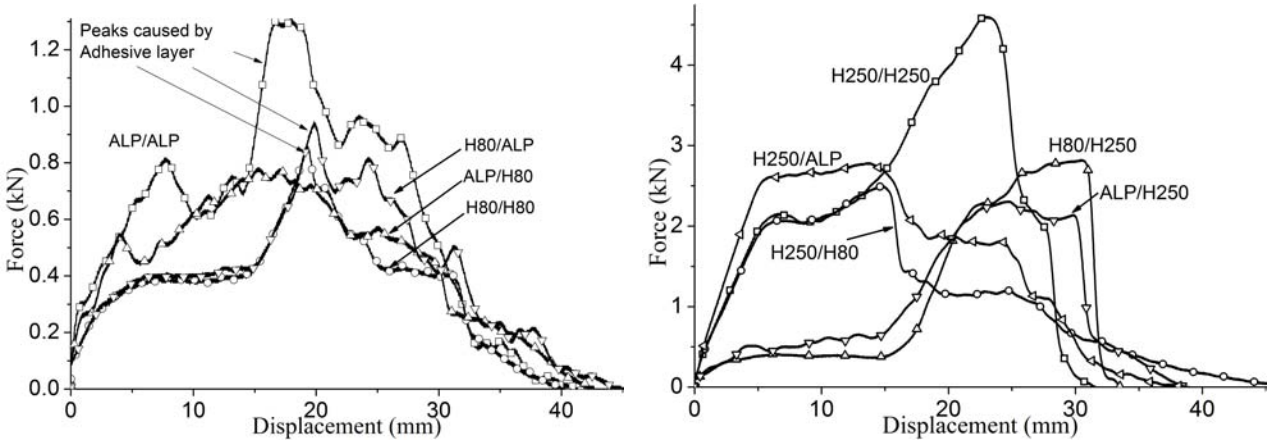

Figure 10: Experimental force-displacement response of bare foams: (a) low yield strength foams and (b) presence dense foam.

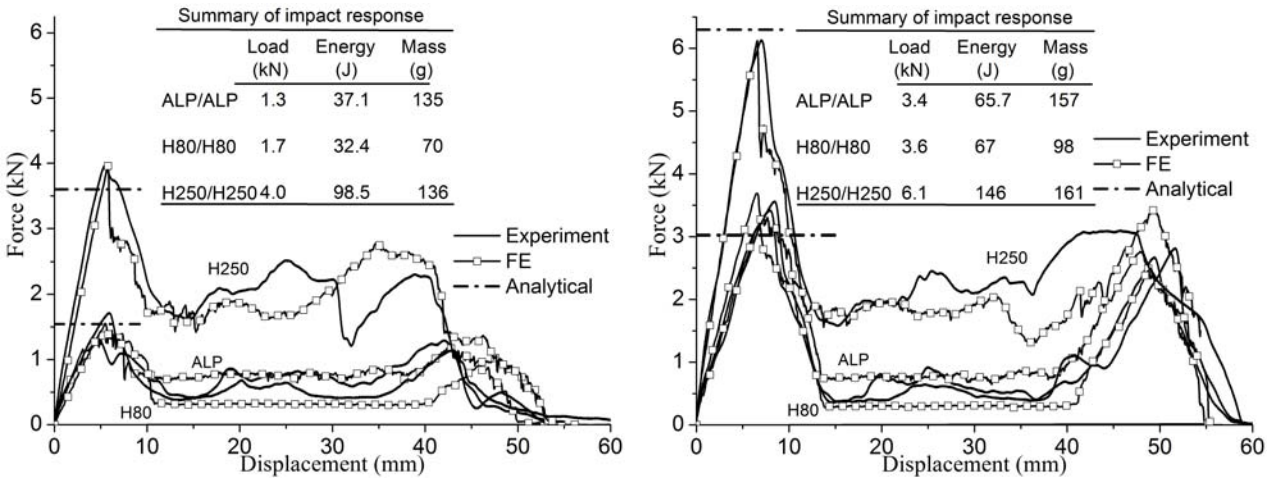

(a) 0.5 mm faceplates

(b) 1.0 mm faceplates

Figure 11: Comparison between experimental, numerical and analytical responses of sandwich plates.

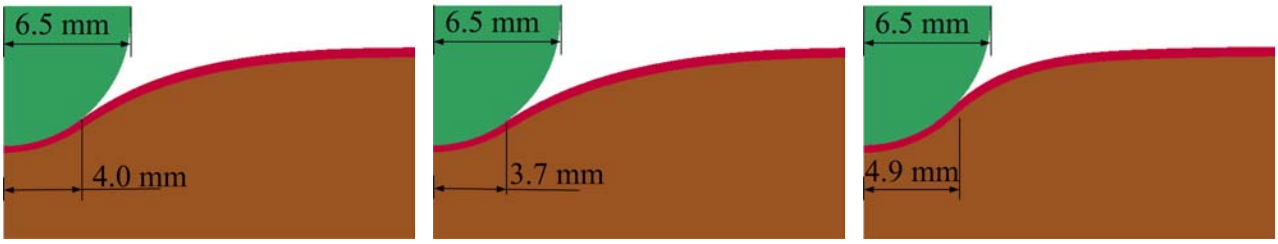

(a) Alporas (b) H80 (c) H250

Figure 12: Effect of sandwich type on the contact radius (just before the face failure or maximum dynamic penetration force for 0.5 mm sandwich plate).

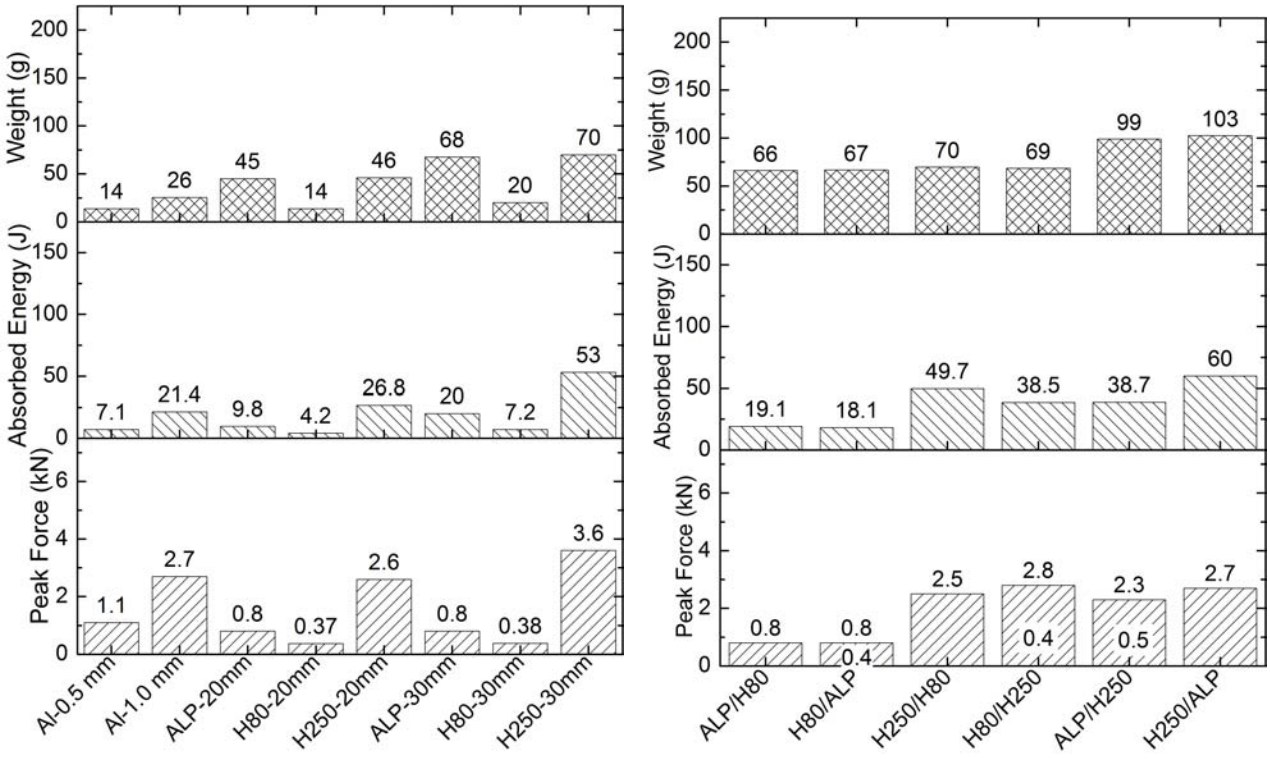

(a) Sandwich constituents

(b) Bare graded foam

Figure 13: Comparison chart of maximum dynamic force, energy absorption and mass of (a) sandwich constituents and (b) bare graded foam.

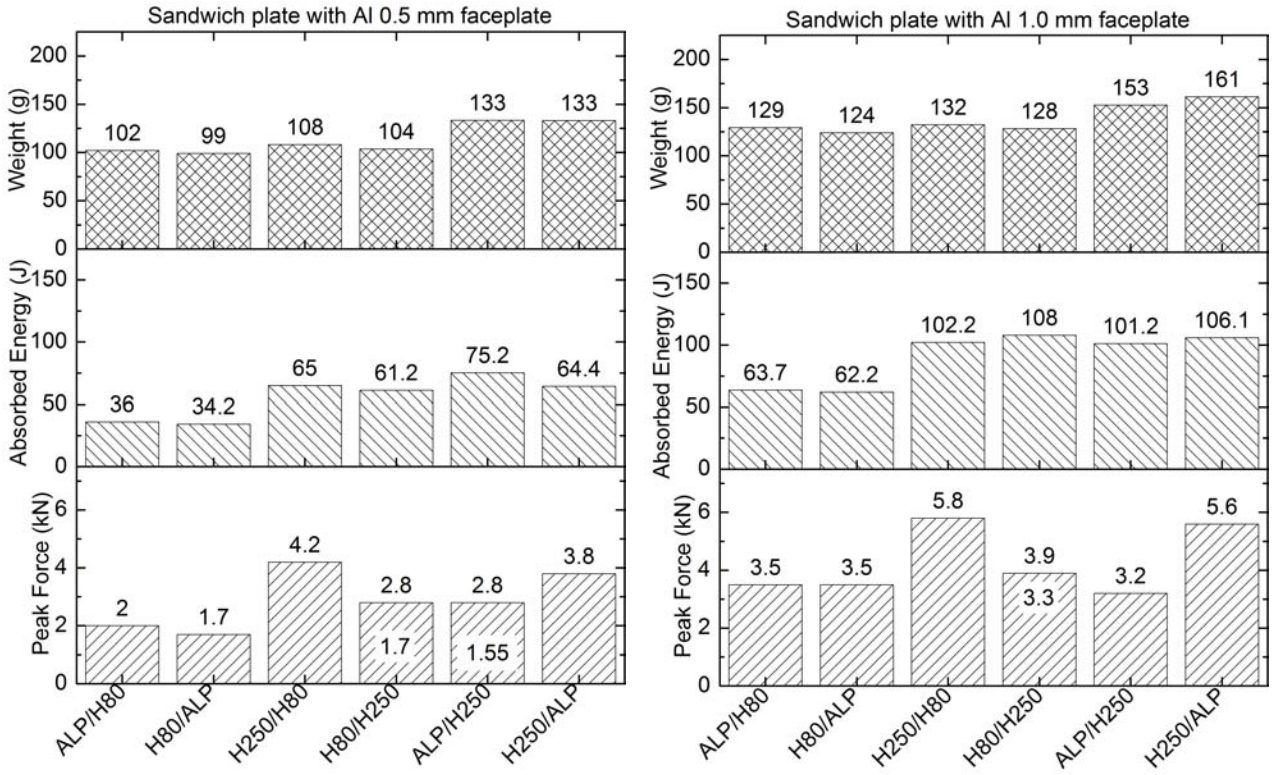

(a) 0.5 mm sandwich plate

(b) 1.0 mm sandwich plate

Figure 14: Comparison chart of maximum dynamic force, energy absorption and mass of (a) 0.5 mm and (b) 1.0 mm.

Table 1: Material properties of aluminum face-plate used in piece-wise linear plasticity constitutive model.

Property	Value
Mass density, ρ_{Al}	2700 kg/m^3
Young's modulus, E_{Al}	70 GPa
Yield stress, $\sigma_{y_{Al}}$ (0.5 mm)	116 MPa
(1.0 mm)	130 MPa
Poisson's ratio, ν_{Al}	0.3
Plastic strain at failure, EPSF (0.5 mm)	0.4
(1.0 mm)	0.5
Effective stress-strain curve	Fig. 2a

Table 2: Material properties of Alporas foam used in honeycomb constitutive model.

Property	Value/Response curve
Mass density, ρ	250 kg/m^3
Young's modulus, $E = E_{AAU} = E_{BBU} = E_{CCU}$	180 MPa
Shear modulus, $G_{ABU} = G_{BCU} = G_{CAU}$	90 MPa
Plastic Poisson's ratio, ν_p	0.0
Yield stress, σ_y	1.5 MPa
Tensile strain at failure, TSEF	0.8
Relative volume at compaction, VF	0.0
Compression stress-strain curve, LCA = LCB = LCC = LCS	Curve (c) in Fig. 3

Table 3: Material properties of Divinycell H80 foam used in honeycomb constitutive model.

Property	Value/Response curve
Mass density, ρ	76 kg/m^3
Young's modulus, $E_{AAU} = E_{BBU}$	30 MPa
Young's modulus, $E = E_{CCU}$	49 MPa
Shear modulus, $G_{ABU} = G_{BCU} = G_{CAU}$	35 MPa
Plastic Poisson's ratio, ν_p	0.0
Yield stress, σ_y	1.2 MPa
Tensile strain at failure, TSEF	0.4
Volumetric strain at failure†, CFAIL	0.1
Relative volume at compaction, VF	0.0
Compression stress-strain curve, LCA = LCB	Curve (e) in Fig. 3
Compression stress-strain curve, LCC = LCS	Curve (d) in Fig. 3

† Volumetric fail strain is incorporated using MAT_ADD_EROSION option.

Table 4: Material properties of Divinycell H250 foam used in honeycomb constitutive model.

Property	Value/Response curve
Mass density, ρ	240 kg/m^3
Young's modulus, E_{AAU}, E_{BBU}	130 MPa, 146 MPa
Young's modulus, $E = E_{CCU}$	175 MPa
Shear modulus, $G_{ABU} = G_{BCU} = G_{CAU}$	116 MPa
Plastic Poisson's ratio, ν_p	0.0
Yield stress, σ_y	6.2 MPa
Tensile strain at failure, TSEF	0.6
Volumetric strain at failure†, CFAIL	0.125
Relative volume at compaction, VF	0.0
Compression stress-strain curve, LCA = LCB	Curve (b) in Fig. 3
Compression stress-strain curve, LCC = LCS	Curve (a) in Fig. 3

† Volumetric fail strain is incorporated using MAT_ADD_EROSION option.